

## Original Article

# Assessment of doxorubicin-induced mouse testicular damage by the novel second-harmonic generation microscopy

Chih-Chao Yang<sup>1\*</sup>, Yen-Ta Chen<sup>2\*</sup>, Chih-Hung Chen<sup>3</sup>, John Y Chiang<sup>4,5</sup>, Yen-Yi Zhen<sup>6,7#</sup>, Hon-Kan Yip<sup>6,7,8,9,10#</sup>

<sup>1</sup>Division of Nephrology, Department of Internal Medicine, Kaohsiung Chang Gung Memorial Hospital and Chang Gung University College of Medicine, Kaohsiung 83301, Taiwan, R.O.C.; <sup>2</sup>Division of Urology, Department of Surgery, Kaohsiung Chang Gung Memorial Hospital and Chang Gung University College of Medicine, Kaohsiung 83301, Taiwan, R.O.C.; <sup>3</sup>Department of Internal Medicine, Kaohsiung Chang Gung Memorial Hospital and Chang Gung University College of Medicine, Kaohsiung 83301, Taiwan, R.O.C.; <sup>4</sup>Department of Computer Science and Engineering, National Sun Yat-Sen University, Kaohsiung 80424, Taiwan, R.O.C.; <sup>5</sup>Department of Healthcare Administration and Medical Informatics, Kaohsiung Medical University, Kaohsiung 80708, Taiwan, R.O.C.; <sup>6</sup>Institute for Translational Research in Biomedicine, Kaohsiung Chang Gung Memorial Hospital, Kaohsiung 83301, Taiwan, R.O.C.; <sup>7</sup>Center for Shockwave Medicine and Tissue Engineering, Kaohsiung Chang Gung Memorial Hospital, Kaohsiung 83301, Taiwan, R.O.C.; <sup>8</sup>Division of Cardiology, Department of Internal Medicine, Kaohsiung Chang Gung Memorial Hospital and Chang Gung University College of Medicine, Kaohsiung 83301, Taiwan, R.O.C.; <sup>9</sup>Department of Medical Research, China Medical University Hospital, China Medical University, Taichung 40402, Taiwan, R.O.C.; <sup>10</sup>Department of Nursing, Asia University, Taichung 41354, Taiwan, R.O.C. \*Equal contributors. #Equal contributors.

Received August 17, 2017; Accepted November 14, 2017; Epub December 15, 2017; Published December 30, 2017

**Abstract:** Microtubules, maintaining a non-linear structure, are suitable for direct observation in living mammalian by second-harmonic imaging microscopy (SHIM) (a new kind of confocal microscopies). Testes constituted by vast seminiferous microtubules (SM), serve as good candidates for visualization by SHIM. This study employs the SHIM and Western-blot (WB) to assess the cellular-molecular levels of doxorubicin (Dox)-induced mouse testicular damage. The SHIM examination was able to clearly identify the integrity of normal architecture of the living mouse testis, namely, the anatomical features of SM, smooth muscle wall of SM, manchette microtubules, exoplasmic microtubules in Sertoli cells and interstitial connective tissue, as well as the destructive feature of SM in Dox-treated mice (n = 6 per group). By day 21 after Dox-treatment, the testicular weight and testicular length were significantly progressively decreased as Dox dosage was stepwise increased, i.e., 0/5/10/15/20 mg/kg/body-weight (BW) (all p<0.0001). The cross-section area of SM was significantly lower in Dox-treated (15 mg/kg-BW) mice than that in controls (p<0.001). The protein expression of vimentin was significantly progressively increased whereas the protein expression of  $\beta$ -tubulin/androgen-receptor was significantly progressively decreased in stepwise increased Dox dosage (all p<0.001). The protein expressions of inflammatory (MMP-9/IL-1 $\beta$ /TNF- $\alpha$ /iNOX), oxidative-stress (NOX-1/NOX-2/NOX-4/oxidized protein), apoptotic (mitochondrial-Bax/cleaved-caspase-3/PARP), fibrotic (Smad3/TGF- $\beta$ ) mitochondrial/DNA-damaged (cytosolic cytochrome-C/ $\gamma$ -H2AX/ATM/KU70), and cell apoptotic/death (PTEN/p53) biomarkers were significantly higher in Dox-treated (15 mg/kg-BW) group than those in controls (all p<0.001). In conclusion, the dose-dependent Dox-caused mouse testicular damage can be not only detected by WB in molecular level but also clearly identified by SHIM in living mice.

**Keywords:** Second-harmonic imaging microscopy, doxorubicin, seminiferous tubule, oxidative stress, apoptosis, inflammation, DNA damage

## Introduction

Advanced chemotherapies for cancer patients have been clearly identified to extend survival and life expectancy, and regrettably, also linked

to increased expectations of adverse effect profile. Of those long term adverse effects of chemotherapies on cancer survivors, infertility has emerged as one of the growing important issues worldwide [1-3].

Doxorubicin (Dox), the Achilles' heel of its clinical application for a wide variety of malignancies, however, is well-known to cause innocent organ/tissue damage due to its cumulative toxicity. In fact, even though Dox induces cancer cell apoptosis, yet at the price of damage testicular germ cells damage [4]. Additionally, Dox has been exhibited to interrupt the sperm maturation, attenuate epididymal sperm concentration, and damage spermatogonial DNA and sperm morphology [5]. The underlying mechanism of Dox contributes its toxic effect on the testis is mainly through oxidative stress/interrupted DNA repair and affecting spermatogenesis and sperm function [6, 7].

In biomaterials, the extracellular matrix, myofibrils, microtubule arrays, and cellulose are non-centrosymmetric structures [8, 9]. These non-centrosymmetric biomaterials have non-linear optical properties of emitting second-harmonic generation (SHG) light [10]. The non-centrosymmetric biomolecules generate new photons with twice the energy and emit twice the frequency by stimulation of halving the wavelength of the initial photons [10, 11]. The nonlinear microscopic optical signal processing in non-centrosymmetric biomolecules is used in second-harmonic imaging microscopy (SHIM) to observe biological organization [12]. Thus, SHIM has potential for wide applications in living biomedical imaging for clinical diagnosis [13-16]. High-resolution non-linear optical imaging for identification of live cells or inside organs by second-harmonic generation (SHG) requires coherent laser light stimulation [15, 17]. The biomolecules hyperpolarizability emissions via SHG are able to project specific cellular organization [16], which has been experimentally applied in cytological testing for clinical diagnoses [10, 18]. To date, SHIM has been applied to monitor colonic cancer progression, evaluate pathological fibrosis, and observe microtubule dynamics [11, 19, 20].

In testes, the cells, including spermatocytes, spermatozoa, spermatids, and Sertoli cells, bear microtubular manchette, spindle microtubules, and axoplasmic microtubules [21-24]. However, to the best of our knowledge, SHIM technique has never been utilized in live observation on cells inside the testes. Accordingly, seminiferous tubules in testis are one kind of microtubule arrays with non-centrosymmetric material [25] that SHIM might be useful for

direct visualization of the specialized microtubule organization in cells within seminiferous tubules. Based on the aforementioned observations and by using an experimental model of Dox-induced mouse testicular damage, the efficacy and acuity of SHIM instrument in assessing the architecture and integrity of mouse testis were performed in the present study.

### Materials and methods

#### *Animals and ethics*

The Institute of Animal Care and Use Committee at Kaohsiung Chang Gung Memorial Hospital approved all animal experimental procedures (Affidavit of Approval of Animal Use Protocol No. 2012052802) which were performed in compliance with the Guide for the Care and Use of Laboratory Animals, 8th edition (NIH publication No. 85-23, National Academy Press, Washington, DC, USA, revised 2011). All animals were accommodated in an animal facility approved by the Association for Assessment and Accreditation of Laboratory Animal Care International (AAALAC) in our hospital with controlled temperature and light cycles (24°C and 12/12 light cycle).

#### *Doxorubicin administration and animal grouping*

For live observation of testicular architecture and integrity by SHIM technique, male adult C57BL/6 (B6) mice (n = 30), weighing 25-30 mg (Charles River Technology, BioLASCO Taiwan Co., Ltd., Taiwan), were equally divided into 5 groups (i.e., n = 6 per group) and received intraperitoneal injection of doxorubicin: 0 mg/kg/2 days, 0.5 mg/kg/2 days, 1.0 mg/kg/2 days, 1.5 mg/kg/2 days, and 2 mg/kg/2 days. Doxorubicin administration was continued for 3 weeks. The mice in the five groups received cumulative doses of doxorubicin at 0 mg/kg, 5 mg/kg, 10 mg/kg, and 15 mg/kg, and 20 mg/kg, respectively. Animals in each group were euthanized by day 21 after finishing the SHIM examination, followed by harvesting the testes for individual study.

For Western blot analysis, additional twelve mice were categorized into sham control (SC) (i.e., received 1.0 cc normal saline/kg/2 days) Dox (i.e., 1.5 mg/kg/2 days)-treated group for 21 days. Thus, the accumulated dose of doxorubicin was 15 mg/kg. Animals in each group

## SHIM to monitor cells in testes

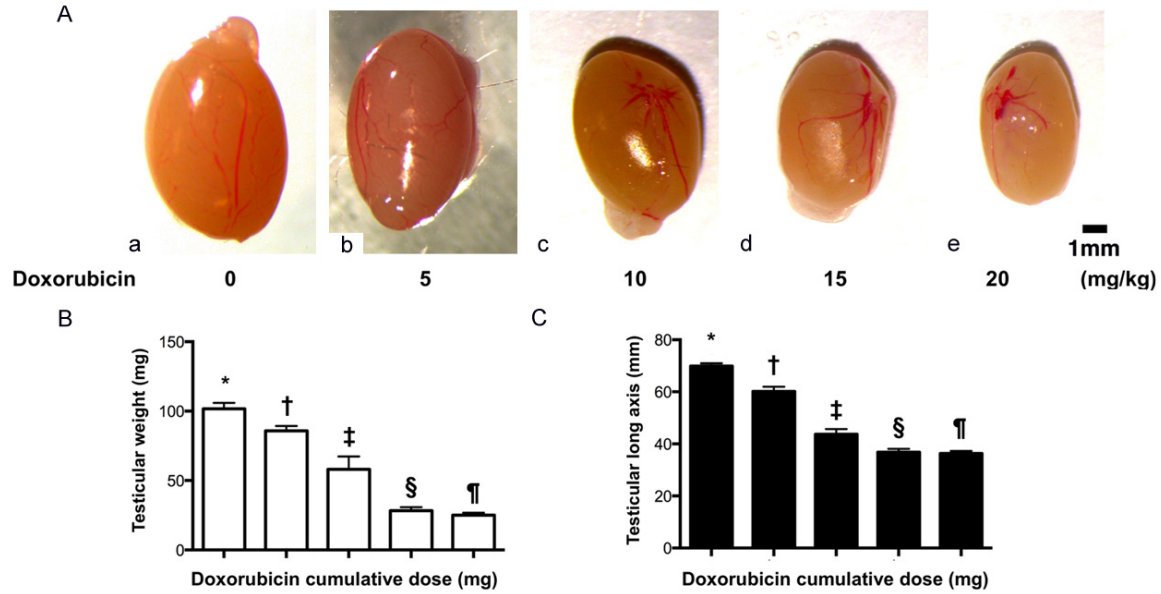


**Figure 1.** Testicular atrophy in doxorubicin-treated mice. A. Illustration of the anatomical feature of testes. As compared with the normal mouse testis (a), the size of doxorubicin-treated mouse testis was progressively reduced as the doxorubicin dose was stepwise increased, i.e., from (b) to (e). B. Analytic result of testicular weight, \* vs. other groups with different (†, ‡, §, ¶),  $p < 0.0001$ . C. Analytical result of testicular long-axis length, \* vs. other groups with different (†, ‡, §, ¶),  $p < 0.0001$ . All statistical analyses were performed by one-way ANOVA, followed by Bonferroni multiple comparison post hoc test ( $n = 6$  for each group). Symbols (\*, †, ‡) indicate significance at the 0.05 level. Doxo = doxorubicin.

were euthanized by day 28, followed by harvested the testes for individually Western blot study.

### *Second-harmonic generation imaging microscopy (SHIM) for visualizing cellular structure in seminiferous tubules of testes*

Mice were anesthetized with 2.0% isoflurane. During multi-photon microscopy (MPM) scanning (FV1000 MPE, Olympus), mice were maintained under anesthesia (a mixture of isoflurane (3.5 L/min) and 100% oxygen (3 L/min)). Room temperature was controlled at 23°C to 25°C, and mice were restrained on heating pads on the MPM platform in a standardized fashion to maintain their body temperature at 37°C. The ventral area was shaved and swabbed with surgical scrub, iodine and alcohol. Upward 1 cm from the base of tail, a 2-3 cm ventral midline skin incision was performed. A single incision of 1-2 cm long was made into the muscle wall. An Olympus FV1000 MPE imaging system was used for all MPM imaging. To apply testes of mice for MPM scanning, one testis was exposed and hydrated with PBS. The testis was then placed under the water immersion objective of the upright microscope for imaging (Olympus, XLPLN 25 × WMP, NA 1.05). The testicular tubules were visualized

using femtosecond pulsed 800 nm light, and the microscopy was focused 20 to 30 mm. Two distinct intrinsic tissue emission signals were collected using photomultiplier tubes [Non De-scanned Detector (NDD)]. The microtubule structures in spermatocytes, spermatids, sperm, and Sertoli cells in the testis were excited using 800 nm light from a tunable femtosecond pulsed Ti-Sapphire laser (Mai Tai Deep See, Spectra-Physics, Newport Corporation). The signals in individual channels were collected as separate grayscale images. Minor adjustments of brightness and color balance were carried out using Adobe Photoshop CS4.

Owing to the non-centrosymmetric character of microtubules, the microtubule organizations in the testicular tubule, i.e., microtubule machettes, spindle microtubules, axoplasmic microtubules and sperm flagella microtubules, are optically able to emit second-harmonic signals. In the present study, the SHIM with multiphoton laser-excitation scanned perpendicularly from the testis surface and optical sectioning was performed with 0.5 μm depth/each increment, i.e., each optical section was 0.5 μm thickness, until there was no SHG signal. The feature of this SHIM could visualize 20 μm deep internal testes in mouse with a cumulative dose of 15 mg/kg doxorubicin and 10 μm

## SHIM to monitor cells in testes

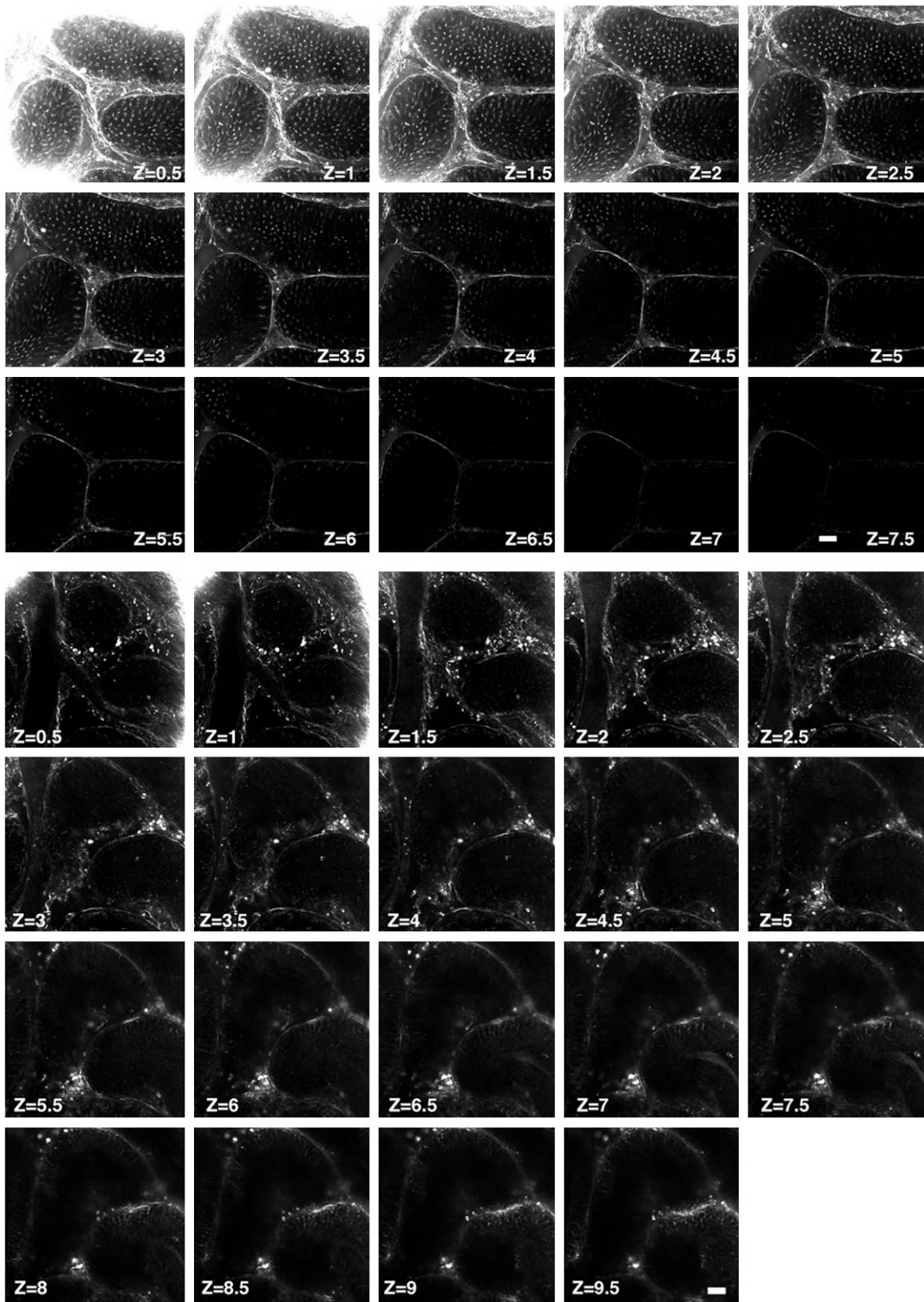


**Figure 2.** Second-harmonic generation microscopy imaging of germ cells in testicular tubules in normal mouse testes. Upper panel: Illustrating the second-harmonic microscopy imaging (SHIM) finding for identification of living normal mouse testes. This second-harmonic generation (SHG) optical sections clearly and consecutively showed the microtubule emitted signals in the seminiferous tubules from superficial to deeper areas. Zone (Z) = 0.5, indi-

## SHIM to monitor cells in testes

cated 0.5  $\mu\text{M}$  and so on,  $Z = 7.5$ , indicated 7.5  $\mu\text{M}$ . Lower panel: Illustrating second-harmonic microscopy imaging (SHIM) finding for identification of living doxorubicin-treated mouse testes. This second-harmonic generation (SHG) optical sections clearly and consecutively showed the microtubule emitted signals in the seminiferous tubules from superficial to more deeper areas. As expected, 15 mg/kg cumulative dose doxorubicin, the seminiferous tubules exhibited much fewer SHG signals in each cross-section area. Zone ( $Z$ ) = 0.5, indicated 0.5  $\mu\text{M}$  and so on,  $Z = 7.5$ , indicated 7.5  $\mu\text{M}$ .

deep internal testes in mouse without doxorubicin treatment; each optical section was 0.5  $\mu\text{m}$  thickness. When scanning probed deep inside the testis, the SHG signals became weaker and was blurred at depth more than 10  $\mu\text{m}$  inside testis, as shown in **Figure 2**. The emission signals were detected as half of the stimulating energy.

### Western blot study

The procedure and protocol for Western blot analysis were based on our previous reports [26, 27]. In brief, equal amounts (50  $\mu\text{g}$ ) of protein extracts were loaded and separated by SDS-PAGE using acrylamide gradients. The membranes were incubated for 1 hour at room temperature with the indicated primary antibodies [mitochondrial Bax (1:1000, Abcam), cleaved poly (ADP-ribose) polymerase (PARP) (1:1000, Cell Signaling), cleaved caspase 3 (1:1000, Cell Signaling), Smad3 (1:1000, Cell Signaling), transforming growth factor (TGF)- $\beta$  (1:500, Abcam), phosphorylation of histone H2AX ( $\gamma$ -H2AX) (1:1000, Cell Signaling), NOX-1 (1:2000, Sigma), NOX-2 (1:500, Sigma), NOX4 (1:1000, Abcam), matrix metalloproteinase (MMP)-9 (1:2000, Abcam), tumor necrosis factor (TNF)- $\alpha$  (1:1000, Cell Signaling), inducible nitric oxide synthase (iNOS) (1:200, Abcam), interleukin (IL)-1 $\beta$  (1:1000, Cell Signaling), phosphorylated (p)-Akt (1:1000, Cell Signaling), ataxia telangiectasia mutated (ATM) (1:2000, Abcam), Ku-70 (1:1000, Cell Signaling), cytosolic cytochrome C (1:2000, BD), mitochondrial (1:2000, BD), peroxisome proliferator-activated receptor gamma coactivator 1-alpha (PGC-1 $\alpha$ ) (1:1000, Abcam), p53 (1:1000, Cell Signaling), Phosphatase and tensin homolog (PTEN) (1:1000, Abcam)]. Horseradish peroxidase-conjugated anti-rabbit immunoglobulin IgG (1:2000, Cell Signaling) was used as a secondary antibody for one hour incubation at room temperature. The washing procedure was repeated eight times within one hour. Immunoreactive bands were visualized by enhanced chemiluminescence (ECL; Amersham Biosciences) and exposed to Biomax L film (Kodak). For the purpose of quantification, ECL signals were digitized using Labwork software (UVP).

### Immunostaining and immunofluorescent (IF) microscopy imaging

An Olympus AX-51 epifluorescence microscope equipped with X-Cite XCT10A (Lumen Dynamics, Wiesbaden, Germany) light source, filters, and 20 $\times$ , 40 $\times$ , 60 $\times$  were used to observe biopsies. Cryosections (6  $\mu\text{m}$ ) from the testes of male mice were prepared for immunostaining and immunofluorescent imaging. The biopsies were fixed in 4% paraformaldehyde in 1 $\times$  PBS buffer for 10 minutes, and permeabilized in 0.5% Triton in 1 $\times$  PBS for 5 minutes. Immunostaining was performed with a monoclonal antibody and secondary antibody Alexa Fluor 488 or Alexa Fluor 546 (Invitrogen). The antibodies used were as follows: vimentin (1:500, Abcam),  $\alpha$ -tubulin (1:500, Santa Cruz Biotechnology),  $\beta$ III-tubulin (1:500, Santa Cruz Biotechnology), and TTC23L (1:1000, Abcam). Additional reagents used were DAPI (1:500, Sigma-Aldrich). Cell nuclei were stained with 0.2  $\mu\text{g}/\text{ml}$  4', 6-diamidino-2-phenylindole (DAPI; Sigma).

### Histochemical examination of testes

Testes were dissected from the abdomen, immersed in 10% formalin for 24 h, and embedded in paraffin. Tissue sections of 5  $\mu\text{m}$  were sliced and stained with H&E for overall morphological evaluation. The specimens with H&E were examined by light microscopy.

### Statistical analysis

Quantitative data are expressed as means  $\pm$  SD. Statistical analysis was adequately performed by ANOVA followed by Bonferroni multiple-comparison post hoc test. SAS statistical software for Windows version 8.2 (SAS institute, Cary, NC) was utilized. A probability value  $<0.05$  was considered statistically significant.

## Results

### Doxorubicin causes testicular atrophy in mice (Figure 1)

Direct microscopic observation of cells in the testes is an ideal way to investigate spermatogenesis and diagnose male infertility. We inve-

## SHIM to monitor cells in testes

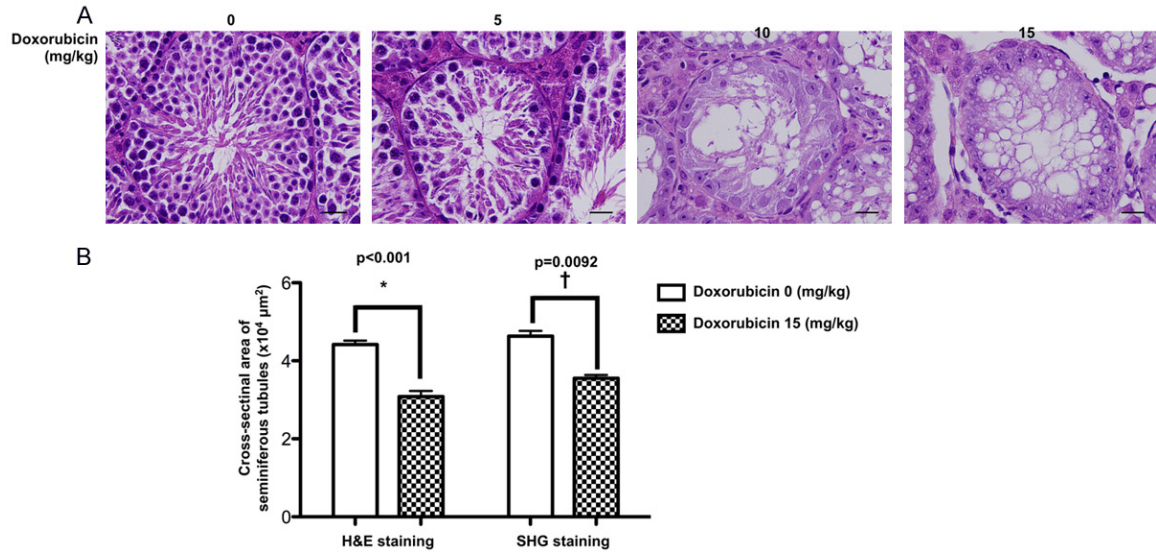


**Figure 3.** Histopathological finding of mouse testicular structure without and with doxorubicin treatment. A. In normal control mouse (i.e., 0 mg/kg Doxo), the microscopy clearly identified the germ cells organized in concentric layers constituting the seminiferous epithelium, tubular lumen, interstitial tissue, interstitial cells in the tubular spaces, spermatogenic lineages and the sertoli cells in seminiferous tubules of testis. On the other hand, the testicular tubules in mouse treated with doxorubicin (5 mg/kg) were identified to have smaller seminiferous tubules and fewer germs cells in the seminiferous tubules than normal control. Additionally, in mouse treated with a higher dose of doxorubicin (10 mg/kg and 15 mg/kg), the testicular tubules were found to be almost disappeared with disorganized seminiferous epithelium. Furthermore, the seminiferous tubules contained only sertoli cells without germ cells. Besides, vacuolization was detected in the seminiferous tubules from 10 mg/kg and 15 mg/kg doxorubicin-treated mice. B. Left bar chart: analytical result of cross-sectional areas of seminiferous tubules assessed by H.E., stain, normal vs. Doxo-treated, \*indicated  $p = 0.0092$ . Right bar chart: analytical results of cross-sectional areas of seminiferous tubules assessed by SHIM imaging, normal vs. Doxo-treated, †indicated  $p < 0.001$ . Data represent the mean of 10 random circular cross-sections  $\pm$  standard error of means (SEM).  $n = 6$  in each group. Doxo = doxorubicin.

stigated the possible use of SHIM for diagnosis of infertility by establishing an infertile mouse model with azoospermia or oligospermia as a negative control. As expected, testicular weight was significantly progressively reduced as the Dox dosage was stepwise increased (i.e., from 0, 5, 10, 15 and 20 mg/kg). Additionally, the length of testicular long axis exhibited an identical trend of testicular weight among the groups.

### Utilization of second-harmonic generation imaging microscopy (SHIM) to examine germ cells in the testicular tube (Figure 2)

As expected, the integrity of the structure in testicular tubule was clearly identified from initial  $0.5 \mu\text{m}$  thickness [i.e., zone (Z) = 0.5] to  $2.5 \mu\text{m}$  thickness (i.e., Z = 2.5). However, when scanning probed placed deeply inside the testis, the SHG signals became weaker and was blurred at depth more than  $7.5 \mu\text{m}$  inside testis.

As compared with healthy mouse, the integrity of testicular architecture in Dox-treated (i.e., 15 mg/kg) mouse was clearly identified to be seriously destroyed. On the other hand, the scanning (i.e., the SHG signals) could probe deeply inside the testis with a clearer visual view in Dox-treated mouse than in healthy mouse. These findings highlighted that SHIM could serve potentially as a simple accessory tool to facilitate clinically semi-quantitative analysis in male patients with malignancy receiving Dox treatment.

### To verify the accurate of SHIM by conventional histopathological method for assessment of seminiferous tubules in doxorubicin-administrated mice (Figure 3)

The H.E. stain demonstrated that as compared with normal control group, the number of seminiferous tubules was significantly and progressively reduced in the stepwise increasing Dox-treated group (i.e., from 0, 5, 10 to 15 mg/kg).

## SHIM to monitor cells in testes

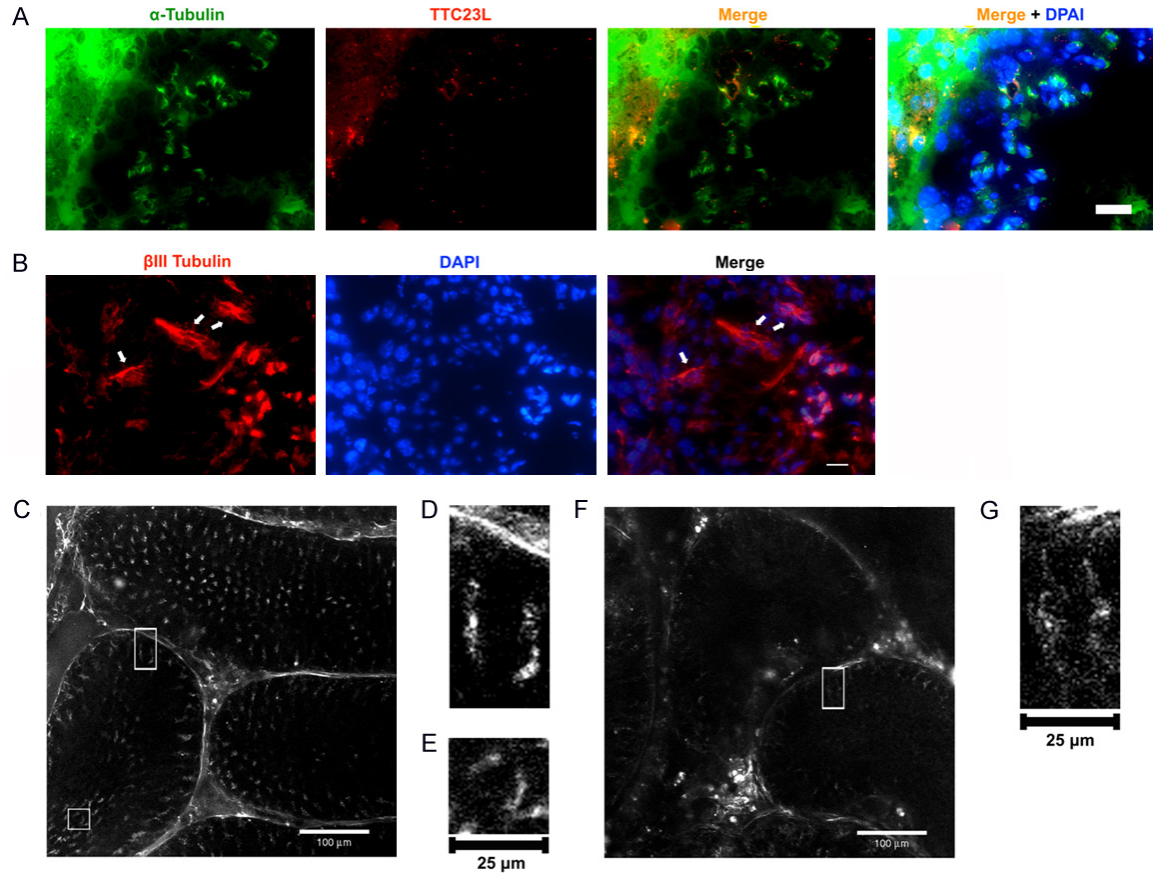


**Figure 4.** Microtubule machettes in spermatids and axoplasmic microtubules in Sertoli cells, and SHIM imaging resolved microtubule structures in sertoli cell and spermatids cells. (A) Immunofluorescent microscopic finding showed the  $\alpha$ -tubulin positive cells in testes. Testis cryosections were stained by  $\alpha$ -tubulin (green) antibody and TTC23L (red) antibody, respectively. The  $\alpha$ -tubulin staining indicated the microtubule machettes in spermatids and TTC23L staining showed a punctuated pattern in spermatids associated with microtubule manchettes. Blue color indicated nuclei stained by DAPI. (B) The anti-beta tubulin III antibody (green) was used as a marker for sertoli cells. The immunostaining of  $\beta$ III-tubulin protein was restricted to Sertoli cells of the seminiferous epithelium. Arrows indicated  $\beta$ III-tubulin antibody (red) staining. Blue color corresponded to nuclei stained by DAPI. Scale bars in right lower corner represent 60  $\mu$ m. (C) SHIM imaging analysis at Z = 3.5  $\mu$ m in testis without doxorubicin treatment displayed microtubule manchette in spermatids and axoplasmic microtubule in sertoli cells. Bar = 100  $\mu$ m. (D) Rectangle in (C) Indicating the area to be selected for high-power magnification shows axoplasmic microtubules. (E) Square in (C) Indicating area to be selected for magnification. The high-power magnification of sub-area showed microtubule manchette. (F) A SHIM imaging analysis at Z = 1  $\mu$ m in testis with doxorubicin treatment displayed only axoplasmic microtubules in sertoli cells to be observed and the microtubule machettes were absent. (G) Rectangle in (F) indicating area to be selected for magnification. The high-power magnification shows axoplasmic microtubules.

Besides, the histopathological finding identified that the number of seminiferous tubules destroyed and disappeared was initially from the central zone of the testis, and then gradually extending into the boundary zone, suggesting the central zone might be a vulnerable zone for Dox-induced testicular damage.

To elucidate the reliability of SHIM for measuring the cross-sectional area of seminiferous tubules in testis, we utilized H.E. microscopic examination, i.e., a standard traditional meth-

od for histopathological analysis, for assessment of cross-sectional area of seminiferous tubules in testis. The results demonstrated that this parameter was significantly higher in normal control group than in Dox-treated (i.e., 15 mg/kg) group in both H.E. microscopic examination and SHIM finding. Additionally, the result of this parameter was comparable between the former and later examinations, highlighting that SHIM can serve reliably as an alternative method for assessing the testis in living mammals.

## SHIM to monitor cells in testes

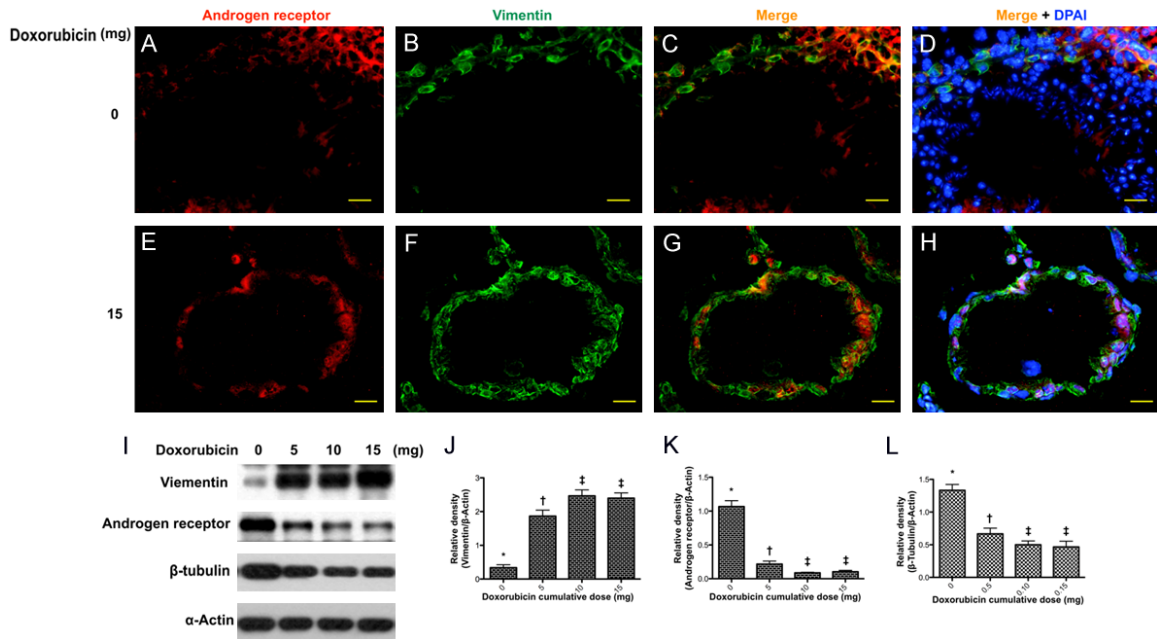


**Figure 5.** Immunostaining and immunoblot of vimentin in sertoli cells. Upper panel: showed the immunofluorescent (IF) findings in situation without doxorubicin treatment. (A and B) Illustrating the IF microscopic finding for identifying the immunostaining of androgen receptor (red) (A) and vimentin in seminiferous tubules (B), respectively. (C and D) Merge IF microscopic finding indicated the Vimentin-positive sertoli cells were present in the seminiferous epithelium. (D) Blue color indicated nuclei stained by DAPI. DAPI-positively stained spermatids and spermatozoa were richly distributed in the seminiferous tubules. Lower panel: showed the IF findings in situation with doxorubicin treatment. (E and F) Illustrating the immunostaining of androgen receptor (red) (E) and vimentin in seminiferous tubules (F), respectively. (G) The IF microscopic finding showed that vimentin-positive sertoli cells were present in the seminiferous epithelium. (H) Blue color indicated nuclei stained by DAPI. No DAPI-stained spermatids and spermatozoa were identified in the seminiferous tubules. Scale bars in right lower corner represent 20  $\mu$ m. (I) Showing Western blot results of sertoli marker vimentin, androgen receptor and  $\beta$ -tubulin, respectively. (J) Protein expression of vimentin, \* vs. other groups with different ( $\dagger$ ,  $\ddagger$ ,  $p < 0.001$ ). (K) Protein expression of androgen receptor (AR), \* vs. other groups with different ( $\dagger$ ,  $\ddagger$ ,  $p < 0.001$ ). (L) Protein expression of  $\beta$ -tubulin, \* vs. other groups with different ( $\dagger$ ,  $\ddagger$ ,  $p < 0.001$ ). All statistical analyses were performed by one-way ANOVA, followed by Bonferroni multiple comparison post hoc test ( $n = 6$  for each group). Symbols (\*,  $\dagger$ ,  $\ddagger$ ) indicate significance at the 0.05 level. Doxo = doxorubicin.

*Spindle microtubules, microtubule machettes and axoplasmic microtubules were clearly identified by SHIM imaging (Figure 4)*

It is well recognized that the microtubule structures can be distinguished by labeling microtubule machettes in spermatids with  $\alpha$ -tubulin antibody and axoplasmic microtubules in Sertoli cells with  $\beta$ III tubulin antibody. In the present study, the IF microscopic finding showed that the  $\alpha$ -tubulin-stained microtubule machettes were present in spermatids and TTC23L protein was punctuated and associated with microtubule machettes. Additionally, the  $\beta$ III tubulin antibody-stained axoplasmic microtubules were present in Sertoli cells.

The SHIM measurement for identifying the testicular structure further showed that in mice

without doxorubicin treatment, the microtubule machettes and axoplasmic microtubules were clearly visible with integrity of architectures. In contrast, while the axoplasmic microtubules were visualized in seminiferous tubules, yet the microtubule machettes were totally absent in those of doxorubicin-treated mice.

*IF microscopic findings for identification of Sertoli cells, spermatids and spermatozoa and protein expressions of vimentin, androgen receptor (AR) and  $\beta$ -tubulin (Figure 5)*

To examine the Sertoli cells in seminiferous tubules, the Sertoli cell marker vimentin was used to label Sertoli cells and DAPI staining was employed to identify the spermatids and spermatozoa. As shown in IF microscopic finding, DAPI-labeled cells were found inside the

## SHIM to monitor cells in testes

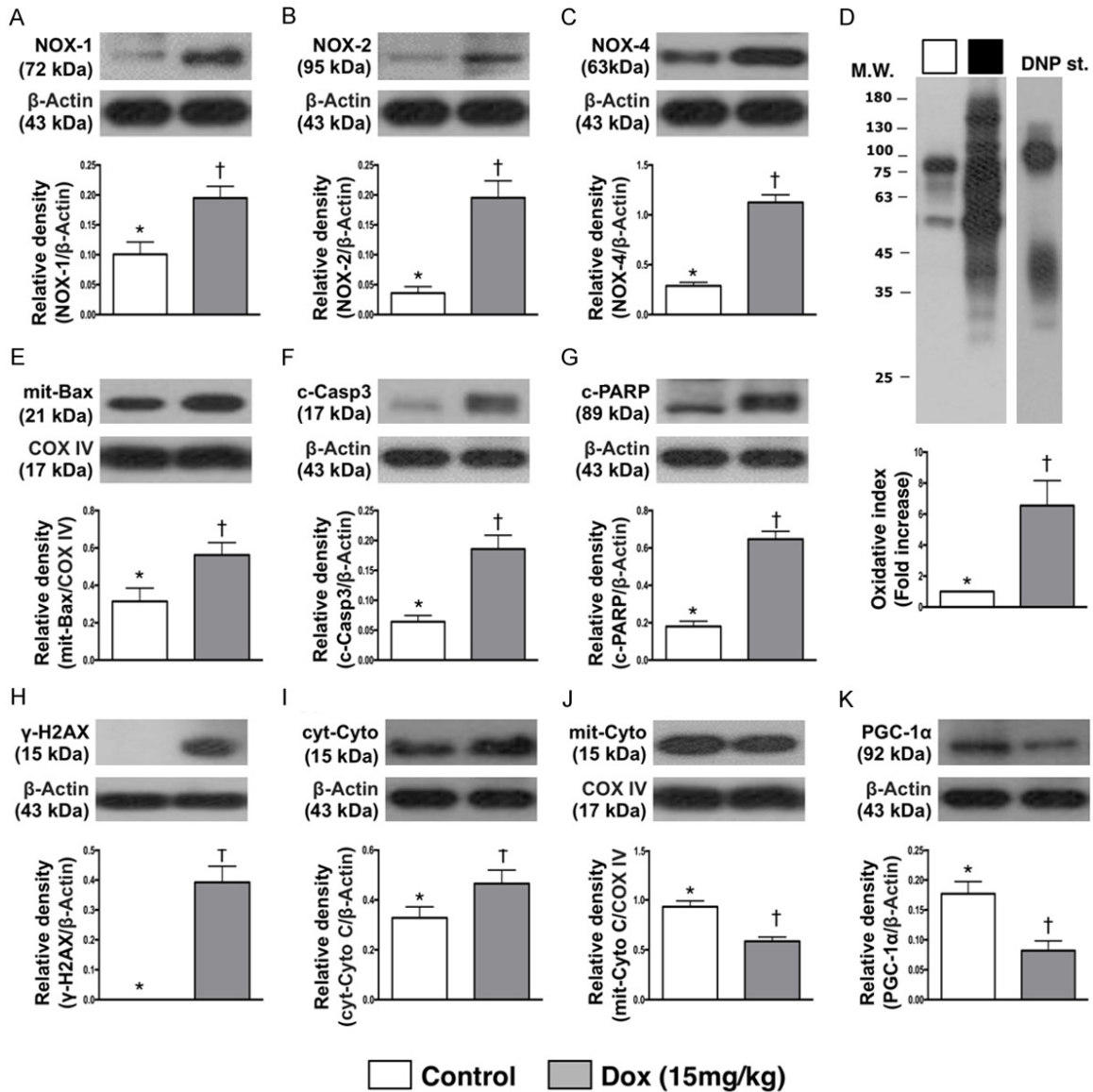


**Figure 6.** Protein expressions of oxidative stress, apoptotic, mitochondrial, DNA-damaged and energy biogenesis biomarkers in testes by day 28 after Dox treatment. A. Protein expression of NOX-1, \* vs. †,  $p < 0.005$ . B. Protein expression of NOX-2, \* vs. †,  $p < 0.001$ . C. Protein expression of NOX-4, \* vs. †,  $p < 0.005$ . D. Oxidized protein expression, \* vs. †,  $p = 0.01$ . (Note: left and right lanes shown on the upper panel represent protein molecular weight marker and control oxidized protein standard, respectively). M.W. = molecular weight; DNP = 1-3 dinitrophenylhydrazine.  $n = 6$  for each group. Dox = doxorubicin (15 mg/kg). E. Protein expression of mitochondrial (mit)-Bax, \* vs. †,  $p < 0.02$ . F. Protein expression of cleaved caspase (c-Casp) 3, \* vs. †,  $p = 0.001$ . G. Protein expression of cleaved poly (ADP-ribose) polymerase (PARP), \* vs. †,  $p < 0.001$ . H. Protein expression of  $\gamma$ -H2AX, \* vs. †,  $p = 0.001$ . I. Protein expression of cytosolic cytochrome (cyt-Cyto) C, \* vs. †,  $p < 0.04$ . J. Protein expression of mitochondrial cytochrome (mit-Cyto) C, \* vs. †,  $p < 0.001$ . K. Protein expression of peroxisome proliferator-activated receptor gamma coactivator 1-alpha (PGC-1 $\alpha$ ),  $p = 0.002$ .  $n = 6$  for each group. Dox = doxorubicin (15 mg/kg).

seminiferous tubule (**Figure 5D**) and vimentin-stained sertoli cells (**Figure 5B**) lining the epithelial layer in seminiferous tubules in the mice without doxorubicin treatment.

In contrast, only vimentin-positive cells (**Figure 5F**) were present in the epithelial layer of seminiferous tubules in mice with a 15 mg/kg cu-

mulative dose of Dox. However, the spermatids and spermatozoa were absent as no DAPI staining was found inside the seminiferous tubules (**Figure 5H**).

The protein expression of vimentin was significantly progressively increased in testicular tissue as the Dox dosage stepwise increased

## SHIM to monitor cells in testes

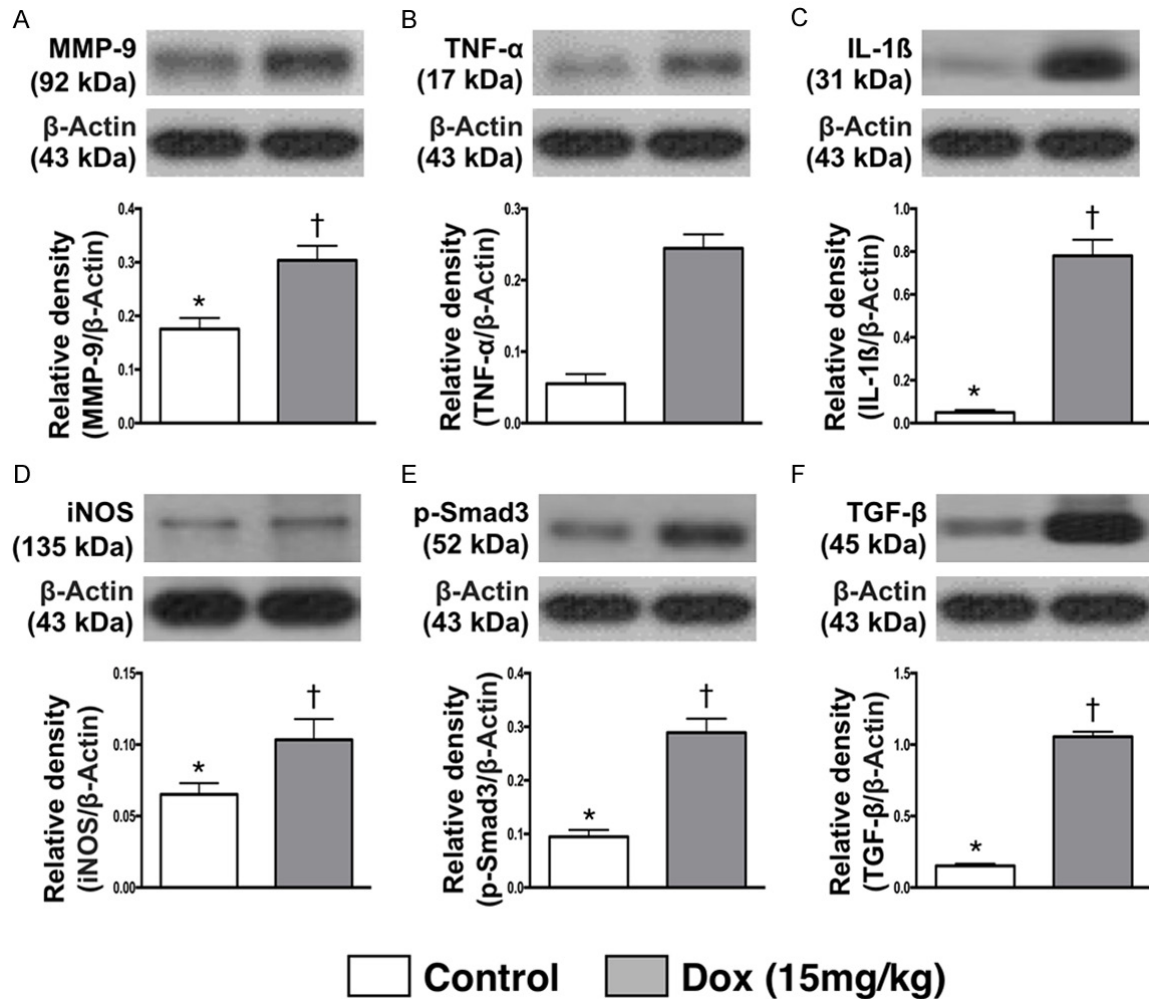


**Figure 7.** Protein expressions of inflammatory and fibrotic biomarkers in testis by day 28 after Dox treatment. A. Protein expressions of matrix metalloproteinase (MMP)-9, \* vs. †,  $p = 0.002$ . B. Protein expression of tumor necrosis factor (TNF)- $\alpha$ , \* vs. †,  $p < 0.001$ . C. Protein expression of interleukin (IL)-1 $\beta$ , \* vs. †,  $p < 0.001$ . D. Protein expression of inducible nitric oxide synthase (iNOS), \* vs. †,  $p < 0.03$ . E. Protein expression of phosphorylated (p)-Samd3, \* vs. †,  $p < 0.001$ . F. Protein expression of transforming growth factor (TGF)- $\beta$ , \* vs. †,  $p < 0.001$ .  $n = 6$  for each group. Dox = doxorubicin (15 mg/kg).

(Figure 5I, 5J), whereas the protein expressions of AR (Figure 5I, 5K) and  $\beta$ -tubulin (Figure 5I, 5L) exhibited an opposite trend of vimentin as the Dox dosage stepwise increased, suggesting that the Western blot analyses were consistent with the data acquired from the IF microscopic findings.

*Protein expressions of oxidative stress, apoptotic, mitochondrial, DNA-damaged and energy biogenesis biomarkers in testis by day 28 after Dox treatment (Figure 6)*

The protein expression of NOX-1, NOX-2 and NOX-4, three indicators of oxidative stress, we-

re significantly higher in Dox-treated (i.e., 15 mg/kg) group than in SC group. Additionally, the oxidized protein expression, another indicator of oxidative stress, exhibited an identical pattern of NOX-1 between two groups.

The protein expression of mitochondrial Bax, cleaved caspase 3 and cleaved PAPP, three indices of apoptosis, exhibited an identical pattern of oxidative stress. Additionally, the protein expression of  $\gamma$ -H2AX, a DNA-damaged indicator, exhibited an identical pattern of apoptosis between the groups. Furthermore, the protein expression of cytosolic cytochrome C, a mitochondrial-damaged indicator, displayed an

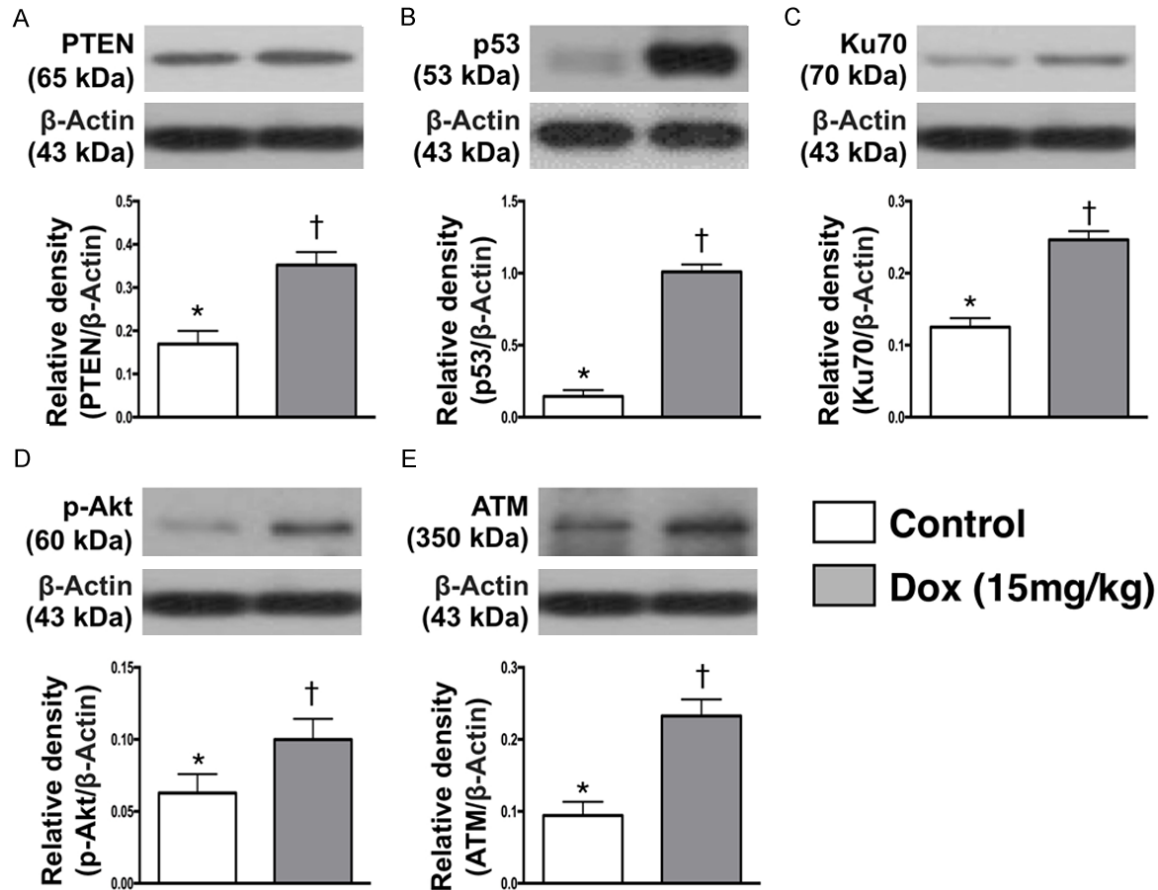


**Figure 8.** Protein expression of cell survival signaling and cell death biomarkers in testis by day 28 after Dox treatment. A. Protein expression of Phosphatase and tensin homolog (PTEN), \* vs. †,  $p < 0.001$ . B. Protein expression of p53, \* vs. †,  $p < 0.001$ . C. Protein expression of Ku70, \* vs. †,  $p < 0.001$ . D. Protein expression of phosphorylated (p)-Akt, \* vs. †,  $p < 0.001$ . E. Protein expression of ataxia telangiectasia mutated (ATM), \* vs. †,  $p < 0.001$ .  $n = 6$  for each group. Dox = doxorubicin (15 mg/kg).

identical pattern of apoptosis. On the other hand, the protein expressions of mitochondrial cytochrome C, an indicator of mitochondrial integrity and PGC-1 $\alpha$ , an indicator of energy biogenesis promotor, showed an opposite pattern of apoptosis between the two groups.

*Protein expressions of inflammatory and fibrotic biomarkers in testis by day 28 after Dox treatment (Figure 7)*

The protein expressions of MMP-9, TNF- $\alpha$ , IL-1 $\beta$  and iNOS, four indicators of inflammation, were significantly higher in Dox-treated animals than SC counterparts. Additionally, the protein expression of phosphorylated (p)-Samd3 and TGF- $\beta$ , two indicators of fibrosis revealed an identical pattern of inflammation.

*Protein expression of cell survival signaling and cell death biomarkers in testis by day 28 after Dox treatment (Figure 8)*

The protein expression of P-TEN, a tumor suppressor protein, was significantly higher in Dox-treated group than in SC one. Additionally, the protein expression of p53, a tumor suppressor protein and a transcription factor that initiates a program of cell cycle arrest, cellular senescence or apoptosis, exhibited an identical pattern of P-TEN between the two groups. Furthermore, protein expression Ku70, an indicator of DNA repair, and p-Akt, an indicator of cellular survival and growth in response to extracellular signals, revealed an identical pattern of P-TEN between the groups. The protein expression of ATM, a stimulator for DNA repair

and blocks cell cycle progression, displayed an identical pattern of P-TEN between the groups.

### Discussion

Although testicular biopsy is routinely performed clinically for the analysis/diagnosis of germ cells in testicular tubes, however, this procedure is invasive to testicular organization [28] which is a very fragile organ, highly susceptible to damage. The aforementioned risk of traditionally invasive means solicits a new and safe accessory modality without invasive procedure, which is paramount important not only to physicians but also to patients. Surprisingly, no current imaging technique (i.e., non-invasive) is available for the examination of cells inside testes in vivo. The most important finding in the present study was that SHIM imaging, non-invasive procedure, clearly identified the macro- and micro-structure of mouse testis as well as both normal and Dox-damaged mouse testicular architectures. Our findings highlight that this is the first study reported to provide a thorough investigation for non-invasively direct visualization of cells in testes in vivo that would be potential for clinical use as well as reproductive study.

Microtubules are non-centrosymmetric biomolecular assemblies. A multi-photon laser technique can activate microtubules in hyperpolarizabilities that can be subsequently observed by second-harmonic microscopy (i.e., SHIM imaging) [9, 13, 20, 28, 29]. An important finding was that as compared with traditional method of testicular biopsy for pathological diagnosis [28], the microtubule structures can be resolved (**Figure 4D, 4E, and 4G**) by the SHIM imaging. In fact, our results showed that SHIM imaging could locate different layers of normal testicular architecture and disease entity (i.e., from superficial and stepwise to deeper layers of testicular structure) rather than only uncertain point of biopsy that provided by traditional method. In this way, this new innovative approach could be viewed as a complementary role of traditional biopsy method for diagnosis of testicular disease.

The clinical uses of Dox are limited due to its dose-dependent adverse effects particularly in cardiac and testicular toxicities [30, 31], resulting in the dilated cardiomyopathy, and spermatogonia fail to differentiate and develop into

spermatocytes, spermatids, and spermatozoa. Additionally, studies have previously identified that azoospermia was frequently observed in patients receiving chemotherapy with doxorubicin [29, 31, 32]. An essential finding in the present study was that by using the SHIM imaging, not only accumulated highest dose (i.e., 20 mg/kg) but also the lowest dose (i.e., 5 mg/kg) of Dox therapy could elicit the damage in the testicular organ/tissue and azoospermia in animals. Accordingly, our findings corroborated with the findings of previous studies [29, 31, 32]. Additionally, immunofluorescent imaging and western blot analysis further confirmed the accuracy of SHIM imaging in observing cytological events deeply within the tissue at high resolution to gain insight into cellular behaviors and molecular signals.

When the molecular level of testicular damage after Dox treatment was examined, we found that the protein expressions of inflammatory, oxidative-stress, apoptotic, fibrotic, DNA-damaged and mitochondrial-damaged biomarkers were substantially higher in Dox-treated group as compared with SC one. On the other hand, the integrities of mitochondrial cytochrome C and PGC-1 $\alpha$  (i.e., two indicators of energy donors for the cells) were remarkably lower in Dox-treated animals than in SC counterparts. Our findings in molecular level, in addition to being comparable with our immunofluorescent results (i.e., cellular level), once again support the accuracy of SHIM imaging for providing the cytological information of testis organ.

An interesting finding in the present study was that those of cell survival suppressing biomarkers (i.e., P-TEN, p53, ATM) and cell survival supporting biomarkers (Ku70, Akt/p-Akt) were all increased in Dox-treated group as compared for NC counterpart. This finding might reflect an intrinsic response of testis to Dox-toxic stimulation for the survival.

### Study limitation

Our study has limitations. First, although SHIM imaging provided attractive and promising images for identification of normal and abnormal testicular structure, it could not provide specific disease entity of testis. Second, this study did not provide an additional treatment group for reversing the Dox-induced testicular damage. Therefore, we could not provide informa-

tion regarding the accurate diagnosis of SHIM imaging for testicular architecture after receiving specific treatment in setting of Dox-induced testicular toxicity.

In conclusion, second-harmonic generation (SHG)-based technologies were applied to provide much more quantitative information on normal or deficient spermatogenesis with a satisfactorily high spatial and temporal resolution.

### Acknowledgements

The authors would like to thank Prof. Samuel H. H. Chan of the Institute for Translational Research in Biomedical Sciences at Kaohsiung Chang Gung Memorial Hospital for his helpful suggestions and use of equipment for acquiring microscopic images. This work was supported by research grants from Chang Gung Memorial Hospital, Chang Gung University (Grant no. CMRPG8B0961 and CMRPG8B0962).

### Disclosure of conflict of interest

None.

**Address correspondence to:** Hon-Kan Yip, Division of Cardiology, Department of Internal Medicine, Kaohsiung Chang Gung Memorial Hospital and Chang Gung University College of Medicine, 123, Dapi Road, Niasung Dist., Kaohsiung 83301, Taiwan, R.O.C. Tel: +886-7-7317123; Fax: +886-7-7322402; E-mail: han.gung@msa.hinet.net

### References

- [1] Marcon L, Hales BF and Robaire B. Reversibility of the effects of subchronic exposure to the cancer chemotherapeutics bleomycin, etoposide, and cisplatin on spermatogenesis, fertility, and progeny outcome in the male rat. *J Androl* 2008; 29: 408-417.
- [2] Meistrich ML. Male gonadal toxicity. *Pediatr Blood Cancer* 2009; 53: 261-266.
- [3] Lee SH and Shin CH. Reduced male fertility in childhood cancer survivors. *Ann Pediatr Endocrinol Metab* 2013; 18: 168-172.
- [4] Hashimoto Y, Terashita K, Niihara T, Yamagishi Y, Ishizaka M, Kanekura K, Chiba T, Yamada M, Kita Y, Aiso S, Matsuoka M and Nishimoto I. Humanin antagonists: mutants that interfere with dimerization inhibit neuroprotection by Humanin. *Eur J Neurosci* 2004; 19: 2356-2364.
- [5] Meistrich ML, van Beek ME, Liang JC, Johnson SL and Lu J. Low levels of chromosomal mutations in germ cells derived from doxorubicin-treated stem spermatogonia in the mouse. *Cancer Res* 1990; 50: 370-374.
- [6] Atessahin A, Turk G, Karahan I, Yilmaz S, Ceribasi AO and Bulmus O. Lycopene prevents adriamycin-induced testicular toxicity in rats. *Fertil Steril* 2006; 85 Suppl 1: 1216-1222.
- [7] Tanigaki R, Sueoka K, Tajima H, Nakabayashi A, Sato K, Asada H, Kato S, Hosoi Y and Yoshimura Y. C-kit expression in spermatogonia damaged by doxorubicin exposure in mice. *J Obstet Gynaecol Res* 2013; 39: 692-700.
- [8] Chen X, Nadiarynkh O, Plotnikov S and Campagnola PJ. Second harmonic generation microscopy for quantitative analysis of collagen fibrillar structure. *Nat Protoc* 2012; 7: 654-669.
- [9] Rivard M, Popov K, Couture CA, Laliberte M, Bertrand-Grenier A, Martin F, Pepin H, Pfeffer CP, Brown C, Ramunno L and Legare F. Imaging the noncentrosymmetric structural organization of tendon with interferometric second harmonic generation microscopy. *J Biophotonics* 2014; 7: 638-646.
- [10] Chen J, Zhuo S, Luo T, Jiang X and Zhao J. Spectral characteristics of autofluorescence and second harmonic generation from ex vivo human skin induced by femtosecond laser and visible lasers. *Scanning* 2006; 28: 319-326.
- [11] Hompland T, Erikson A, Lindgren M, Lindmo T and de Lange Davies C. Second-harmonic generation in collagen as a potential cancer diagnostic parameter. *J Biomed Opt* 2008; 13: 054050.
- [12] Zipfel WR, Williams RM, Christie R, Nikitin AY, Hyman BT and Webb WW. Live tissue intrinsic emission microscopy using multiphoton-excited native fluorescence and second harmonic generation. *Proc Natl Acad Sci U S A* 2003; 100: 7075-7080.
- [13] Campagnola P. Second harmonic generation imaging microscopy: applications to diseases diagnostics. *Anal Chem* 2011; 83: 3224-3231.
- [14] del Barco O and Bueno JM. Second harmonic generation signal in collagen fibers: role of polarization, numerical aperture, and wavelength. *J Biomed Opt* 2012; 17: 045005.
- [15] He B, Wu JP, Kirk TB, Carrino JA, Xiang C and Xu J. High-resolution measurements of the multilayer ultra-structure of articular cartilage and their translational potential. *Arthritis Res Ther* 2014; 16: 205.
- [16] Sun W, Chang S, Tai DC, Tan N, Xiao G, Tang H and Yu H. Nonlinear optical microscopy: use of second harmonic generation and two-photon microscopy for automated quantitative liver fibrosis studies. *J Biomed Opt* 2008; 13: 064010.
- [17] Zoumi A, Yeh A and Tromberg BJ. Imaging cells and extracellular matrix in vivo by using sec-

## SHIM to monitor cells in testes

- ond-harmonic generation and two-photon excited fluorescence. *Proc Natl Acad Sci U S A* 2002; 99: 11014-11019.
- [18] Williams RM, Zipfel WR and Webb WW. Interpreting second-harmonic generation images of collagen I fibrils. *Biophys J* 2005; 88: 1377-1386.
- [19] Keikhosravi A, Bredfeldt JS, Sagar AK and Eliceiri KW. Second-harmonic generation imaging of cancer. *Methods Cell Biol* 2014; 123: 531-546.
- [20] Yu CH, Langowitz N, Wu HY, Farhadifar R, Bruges J, Yoo TY and Needleman D. Measuring microtubule polarity in spindles with second-harmonic generation. *Biophys J* 2014; 106: 1578-1587.
- [21] Correa LM, Nakai M, Strandgaard CS, Hess RA and Miller MG. Microtubules of the mouse testis exhibit differential sensitivity to the microtubule disruptors carbendazim and colchicine. *Toxicol Sci* 2002; 69: 175-182.
- [22] Neely MD and Boekelheide K. Sertoli cell processes have axoplasmic features: an ordered microtubule distribution and an abundant high molecular weight microtubule-associated protein (cytoplasmic dynein). *J Cell Biol* 1988; 107: 1767-1776.
- [23] Smith LB, Milne L, Nelson N, Eddie S, Brown P, Atanassova N, O'Bryan MK, O'Donnell L, Rhodes J, Wells S, Napper D, Nolan P, Lalanne Z, Cheeseman M and Peters J. *KATNAL1* regulation of sertoli cell microtubule dynamics is essential for spermiogenesis and male fertility. *PLoS Genet* 2012; 8: e1002697.
- [24] Akhmanova A, Mausset-Bonnefont AL, van Cappellen W, Keijzer N, Hoogenraad CC, Stepanova T, Drabek K, van der Wees J, Mommaas M, Onderwater J, van der Meulen H, Tanenbaum ME, Medema RH, Hoogerbrugge J, Vreeburg J, Uringa EJ, Grootegoed JA, Grosveld F and Galjart N. The microtubule plus-end-tracking protein CLIP-170 associates with the spermatid manchette and is essential for spermatogenesis. *Genes Dev* 2005; 19: 2501-2515.
- [25] Dombeck DA, Kasischke KA, Vishwasrao HD, Ingelsson M, Hyman BT and Webb WW. Uniform polarity microtubule assemblies imaged in native brain tissue by second-harmonic generation microscopy. *Proc Natl Acad Sci U S A* 2003; 100: 7081-7086.
- [26] Chen HH, Chen YT, Yang CC, Chen KH, Sung PH, Chiang HJ, Chen CH, Chua S, Chung SY, Chen YL, Huang TH, Kao GS, Chen SY, Lee MS and Yip HK. Melatonin pretreatment enhances the therapeutic effects of exogenous mitochondria against hepatic ischemia-reperfusion injury in rats through suppression of mitochondrial permeability transition. *J Pineal Res* 2016; 61: 52-68.
- [27] Chua S, Lee FY, Chiang HJ, Chen KH, Lu HI, Chen YT, Yang CC, Lin KC, Chen YL, Kao GS, Chen CH, Chang HW and Yip HK. The cardioprotective effect of melatonin and exendin-4 treatment in a rat model of cardiorenal syndrome. *J Pineal Res* 2016; 61: 438-456.
- [28] Cerilli LA, Kuang W and Rogers D. A practical approach to testicular biopsy interpretation for male infertility. *Arch Pathol Lab Med* 2010; 134: 1197-1204.
- [29] Stoothoff WH, Bacskai BJ and Hyman BT. Monitoring tau-tubulin interactions utilizing second harmonic generation in living neurons. *J Biomed Opt* 2008; 13: 064039.
- [30] Chatterjee K, Zhang J, Honbo N and Karliner JS. Doxorubicin cardiomyopathy. *Cardiology* 2010; 115: 155-162.
- [31] Ward JA, Bardin CW, Knight M, Robinson J, Gunsalus G and Morris ID. Delayed effects of doxorubicin on spermatogenesis and endocrine function in rats. *Reprod Toxicol* 1988; 2: 117-126.
- [32] Suter L, Bobadilla M, Koch E and Bechter R. Flow cytometric evaluation of the effects of doxorubicin on rat spermatogenesis. *Reprod Toxicol* 1997; 11: 521-531.